Multi-wavelength Laser Backscatter Measurements of LOX-Kerosene Rocket Plumes

February 1999

Dr. John Stryjewski
Andrew Grunke
Joseph Salg
Nichols Research Corporation
Brad Griffis
Computer Sciences Raytheon
Michael Lovern
SPAWARSYSCEN San Diego

ABSTRACT

The Ballistic Missile Defense Organization's (BMDO) Innovative Science and Technology Experimentation Facility (ISTEF[1]) is located on the Kennedy Space Center at Cape Canaveral Florida. The ISTEF conducts research and development in the area of passive and active electro-optical science and technology for missile defense and its location provides a unique opportunity to observe a large number of rocket launches. Atlas II first stage engines use LOX-kerosene as the propellant and are representative of a number of tactical and theater ballistic missiles. Incomplete (non-stochiometric) combustion of LOX-kerosene leads to soot formation, the presence of which could be a useful threat discriminant or identifier. The concentration and size of the soot particles is extremely important when modeling the signature from LOX-kerosene plumes[2]. Previously[3], ISTEF measured the laser radar cross sections of LOX-kerosene plumes in the visible and NIR. This paper reports the results of follow-on measurements, which greatly improve the accuracy and sensitivity of the previous measurements. To our knowledge these are the only multi-wavelength, in-situ measurements of laser-radar cross sections of LOX-kerosene plumes. Absolute (calibrated) laser radar cross sections of both the plume and hardbody were measured at wavelengths of 532nm and 1064nm simultaneously at altitudes ranging from 1km to 20km. Significant variation between the visible and NIR laser radar cross sections as a function of altitude was measured which implies that the particle size distribution has a strong dependence on altitude. The laser illuminator was a frequency doubled pulsed Nd:YAG transmitting at both 532nm and 1064nm with a pulse width of 10ns and repetition rate of 10Hz, and the laser backscatter receiver was a 0.5 meter telescope with APD detectors.

---

1 SPAWARSYSCEN San Diego manages the ISTEF program for BMDO and Nichols Research Corporation is the on-site contractor.
2 "Revised Predictions of Laser Transmission and Reflectance for Delta and Atlas Plumes", Tech. Rep. for BMDO contract F08650-92-C-0064
3 "In Situ Measurements of Soot Formation in Atlas Rocket Plumes", pub. in the proceeding of the 97' Active IRIS Meeting.

Form SF298 Citation Data

Report Date *("DD MON YYYY")* 00021999	**Report Type** N/A	**Dates Covered (from... to)** *("DD MON YYYY")*

Title and Subtitle Multi-wavelength Laser Backscatter Measurements of LOX-Kerosene Rocket Plumes	**Contract or Grant Number**
	Program Element Number
Authors	**Project Number**
	Task Number
	Work Unit Number
Performing Organization Name(s) and Address(es) Nichols Research Corporation	**Performing Organization Number(s)**
Sponsoring/Monitoring Agency Name(s) and Address(es)	**Monitoring Agency Acronym**
	Monitoring Agency Report Number(s)
Distribution/Availability Statement Approved for public release, distribution unlimited	
Supplementary Notes	
Abstract	
Subject Terms	
Document Classification unclassified	**Classification of SF298** unclassified
Classification of Abstract unclassified	**Limitation of Abstract** unlimited
Number of Pages 20	

1. Introduction

The Ballistic Missile Defense Organization (BMDO) maintains the Innovative Science and Technology Experimentation Facility (BMDO/ISTEF) at the Kennedy Space Center in Florida. This site is adjacent to the Cape Canaveral Air Force Station (CCAFS) space launch facility. This location provides us with a large number of targets of opportunity; offering a rich testbed of surrogate TMD and NMD treat representative targets. Among these targets are the LOX-kerosene Atlas and the combined LOX-kerosene/solid-propellant Atlas, Delta, the Hypergolic/solid-propellant fueled Titan rockets and the all solid propellant Athena (peace keeper) rocket. BMDO/ISTEF regularly observes these launches with both active and passive sensors to support BMDO and other DOD programs. These sensors are hosted on any of a number of fixed and transportable tracking mounts.

In the past few years there has been considerable interest in the signatures, both active and passive, associated with liquid propellant rockets. In particular, in the wake of Desert Storm and the proliferation of SCUD class missiles to third world governments such as Korea, Pakistan and Iran, there is a heightened interest in the LOX-Kerosene propellant rockets.

ISTEF is currently engaged in a measurements program aimed at providing data on the chemical and particulate (soot) make-up of LOX-kerosene plumes. These data are of interest not only to the plume phenominologists but also to those groups interested in booster typing and aim point selection.

In particular ISTEF has been working with Aero-Optics Incorporated (AOI) and the Institute for Defense Analysis (IDA) to measure the active and passive signature of the LOX-kerosene plumes of Atlas rockets. The passive measurements cover wavebands from UV to LWIR and the active sensors measure the Laser Radar Cross Section (LRCS) of the plume at 532nm and 1064nm. It is these active LRCS measurements which are the main concern of this paper. We will discuss two of these data collections. The first mission, (henceforth referred to as, the “First Experiment”) was our first active data collection on a boosting Atlas rocket. The *passive* sensors on this mission were calibrated metrically but not radiometrically. After a hiatus of several years the question of soot distribution and soot particle size was again revisited with the ISTEF active sensors. The laser system used on this second mission (henceforth referred to as, the “Second Experiment”) was much improved in sensitivity compared to the First Experiment. Finally, calibrated UV, MWIR and LWIR passive FPAs were added to the setup for the Second Experiment.

The First Experiment (Eastern range OPNR A0116) was conducted on July 31, 1995 when an Atlas II rocket was launched from launch complex 36 at the Cape Canaveral Air Force Station. This rocket had a pure LOX-Kerosene first stage. We illuminated the hardbody and plume of this rocket with a 1 joule class, Q-switched, Nd:YAG laser and measured the reflectance of both the hardbody and the plume at altitudes between 1km and 30km.

The Second Experiment (Eastern range OPNR A7050) was conducted on March 16, 1998 when an Atlas II rocket was launched from the Cape Canaveral Air Force Station. This rocket also had a pure LOX-Kerosene first stage. We again illuminated the hardbody and plume of this rocket with a 1 joule class, Q-switched, Nd:YAG laser and measured the reflectance of both the hardbody and the plume at altitudes between 1km and 20km.

In this paper our goal is to convey the high quality and comprehensive nature of these two data sets and to describe the utility of this data to both the plume modeling and the target signature communities. Finally, as you read this paper, we hope that the advantage of complementary active and passive data sets will be apparent.

2. The First Experiment

The goal of the First Experiment was to measure the LRCS of the plume of a boosting Atlas rocket as a function of altitude at both 532nm and 1064nm. This was done by tracking a point approximately 30m from the engine nozzles as the rocket boosted. Additionally, when the rocket reached an altitude of approximately 12km the laser beam was scanned from the nozzle plane to several hundred meters below the nozzles. Also, at two points during the track, the laser beam was scanned onto the rocket hardbody to aid in the atmospheric calibration.

Metrically calibrated passive FPA data were collected to complete the angle-angle-range solution for the target positions

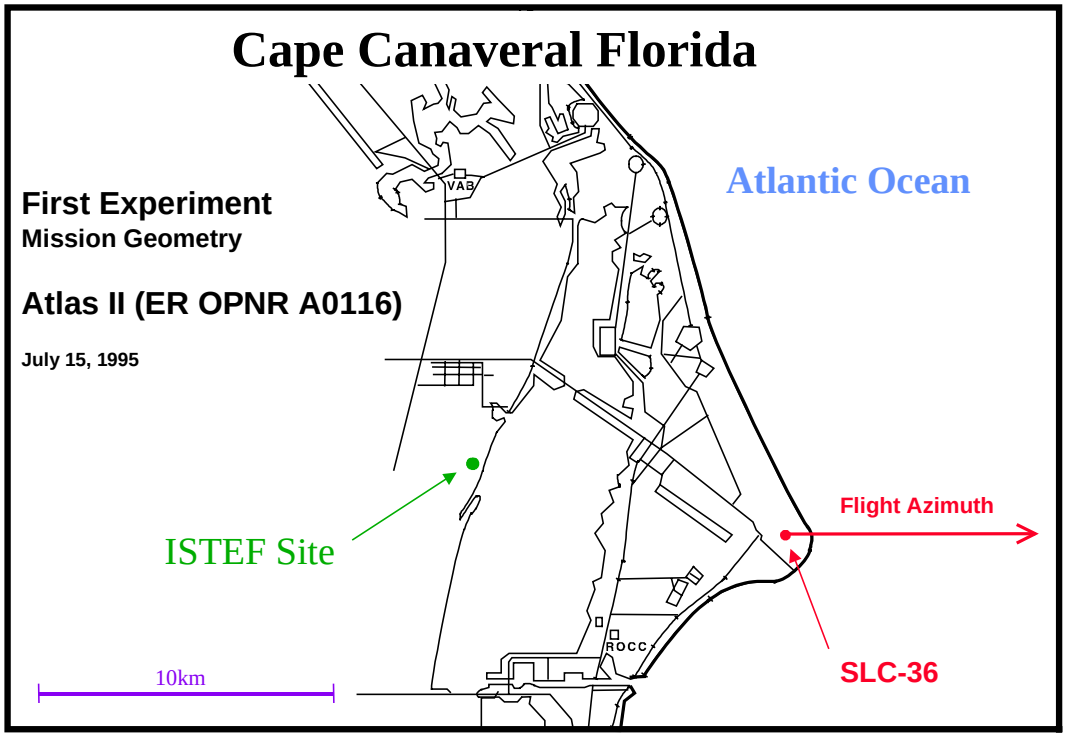

Figure 1 - Mission Geometry for First Mission

2.1. The Location

Figure 1 shows the launch geometry for the First Experiment. The laser and passive sensors were located at the ISTEF site, which is at a distance of approximately 10km from the launch point. The Atlas rocket flew eastward away from the ISTEF. This limited the length of the data collection since the rocket was at nearly 180 degrees aspect after about 120 TALO.

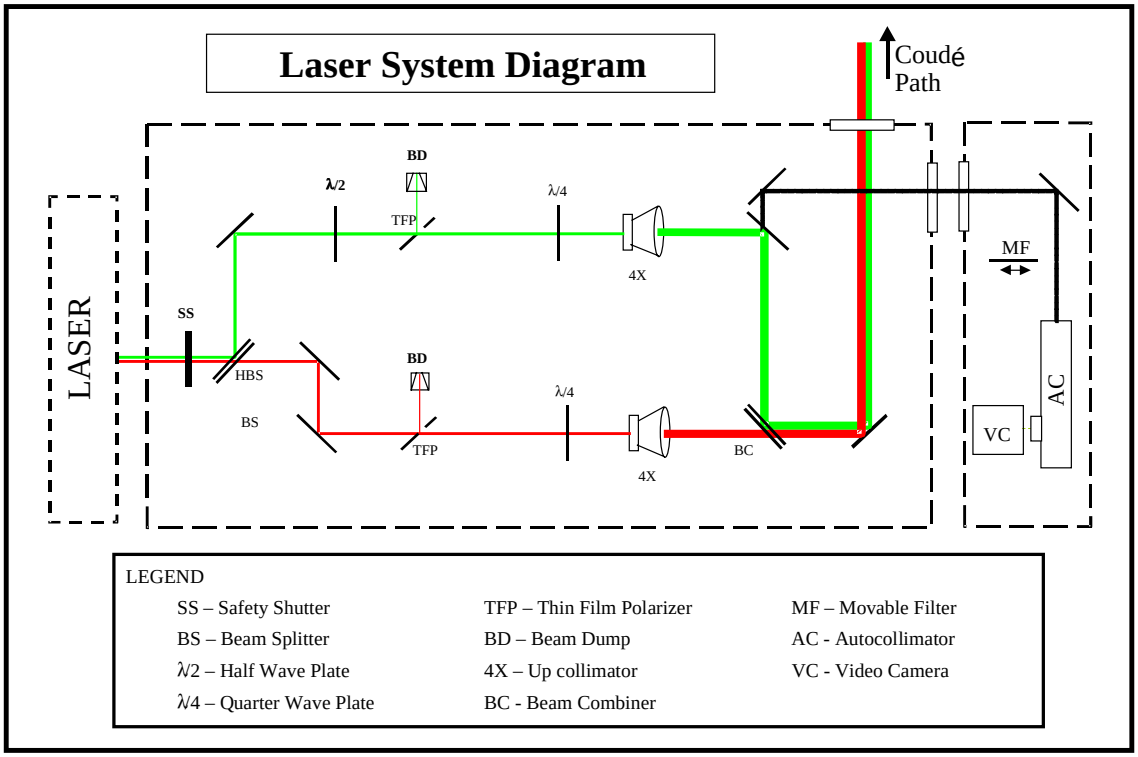

Figure 2 - Laser System Diagram

2.2. The Laser System

The hardware consists of three parts: the laser transmitter, the avalanche photo-diode based receiver-detector and a PC based digital recording system.

2.2.1. The Transmitter

The laser transmitter is a Continuum, 1 joule Nd:YAG laser. It has a 10Hz repetition rate and a 10ns pulse width. A frequency doubler is installed to transmit at frequencies of 532nm and 1064nm

simultaneously. Additional optics are included (Figure 2) to independently control the divergence, power and polarization of the laser output. For the First experiment the laser divergence was set to 250 microradians for both the 532nm and 1064nm beams. Also, the polarization was right circularly polarized for both beams. The transmitted power was 0.45 J/pulse at 532m and 0.12J/pulse at 1064nm.

The laser is housed in a laboratory building and is transmitted via a mirror path to the coude feed of the ISTEF Graz Tracking mount (Figures 3,4).

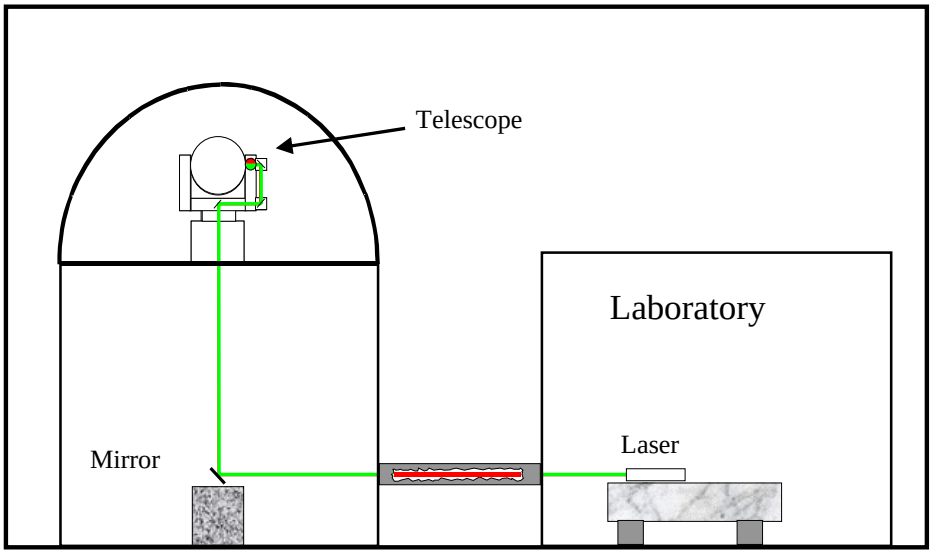

Figure 3 - Coude Feed

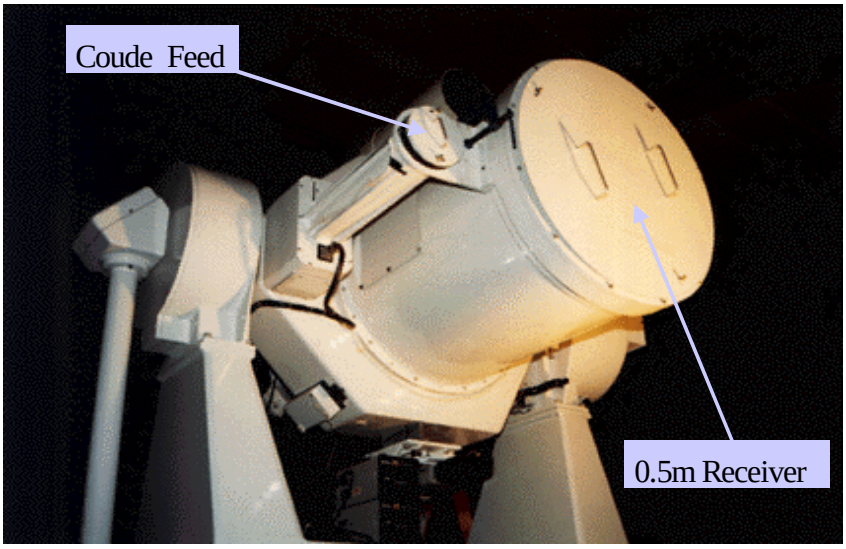

Figure 4 - ISTEF GRAZ Mount

2.2.2. The Receiver

The receiver is a 1/2 meter Cassegrain telescope (Figure 3). 5% of the light gathered by the telescope is focused onto a boresight camera and the remaining 95% is launched into a 400 micron optical fiber which transfers it to an environmentally controlled laboratory where the detectors reside. The detectors are Avalanche Photodiodes (APDs). The 532nm light is measured using a standard Si APD and the l064nm light is measured using an enhanced Si APD. The system is set up so that it can simultaneously measure both the visible and NIR signals.

A fiber optic attenuator (Figure 5) was used to include control the irradiance on the APDs. This was necessary do to the large variance (up to 6 orders of magnitude) in the backscattered signal measured during launches.

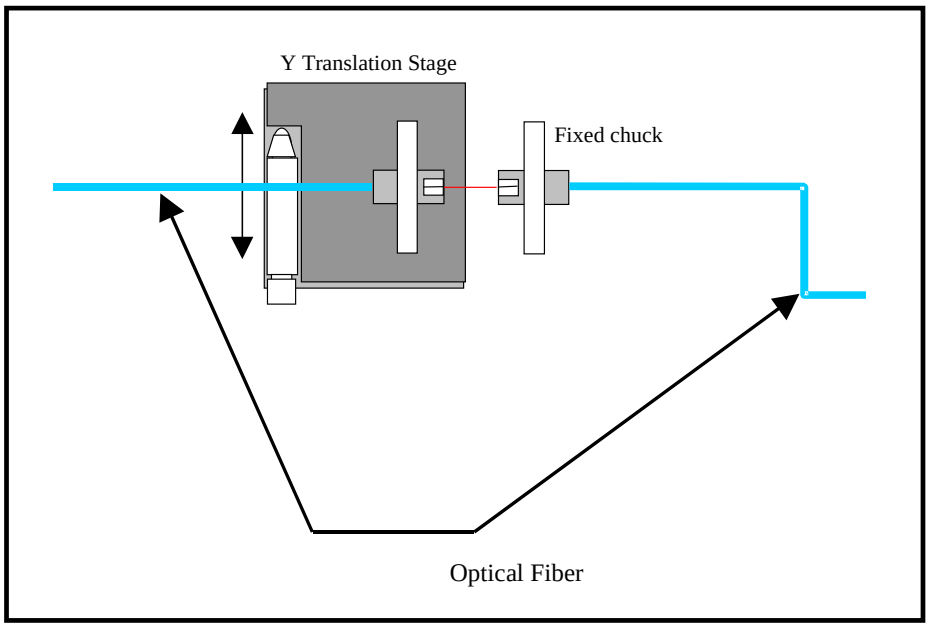

Figure 5 - Fiber Optic Attenuator

2.2.3. The Data Recording System

The signals detected by the APDs are digitized using a high-speed digitizing oscilloscope. The temporal traces from these signals are read from the digitizer and stored on a PC hard drive, in real time. Each backscatter signal was digitized at 8 bits deep and at a rate of 500Mhz.

In addition to the laser backscatter returns, the tracking mount pointing angles, fiber optic attenuator settings and target range were also recorded in real time.

2.2.4. Calibration

The response of the laser backscatter receiver was calibrated using reflectance measurements from a Spectralon reference target. Measurements were taken in the laboratory and on the ISTEF 1km Laser Test Range.

2.3. The Passive Sensors Complement

On the First Experiment, the GRAZ (Figure 4) tracking mount was outfitted with an array of visible cameras. The characteristics of these sensors are shown in Table 1. These sensors were not radiometrically calibrated, however the were *metrically* calibrated to provide good angle-angle data so the 3D position of the target could be determined. All cameras were recorded on SVHS tape, which was encoded with IRIG B (UTC) time on one audio channel.

OPTIC	APERTURE	FOCAL LENGTH	CAMERA	BANDPASS
GRAZ Main	20”	480”	Xybion ICCD	visible
Zoomar	5”	40”	Panasonic CCD	532nm (3nm notch filter)
Meade	8”	80”	Panasonic CCD	532nm (3nm notch filter)
Wide Angle	2”	8”	Sony CCD	visible

Table 1 – Passive Cameras for First Experiment

On the Second Experiment, as described below, we added a second tracking mount and *radiometrically* calibrated LWIR, MWIR, NIR and UV cameras.

3. The Second Experiment

The overall goal of the Seconds Experiment was the same as the First Experiment namely, to measure the LRCS of the plume of a boosting Atlas rocket as a function of altitude at both 532nm and 1064nm. However, a number of improvements to the experimental setup were implemented. Most notable was the inclusion of radiometrically calibrated LWIR, MWIR, NIR and UV imaging cameras. These were hosted on a second tracking mount, which was placed 28km from the launch site, so that it looked approximately at right angles to the mount with the laser.

Just as in the First Experiment the laser tracked a point approximately 10m from the engine nozzles as the rocket boosted. Additionally, at several points during the track, the laser beam was scanned onto the rocket hardbody to aid in the atmospheric calibration. Finally, both tracking mounts collected metrically, calibrated passive FPA data to complete the angle-angle-range solution for the target positions.

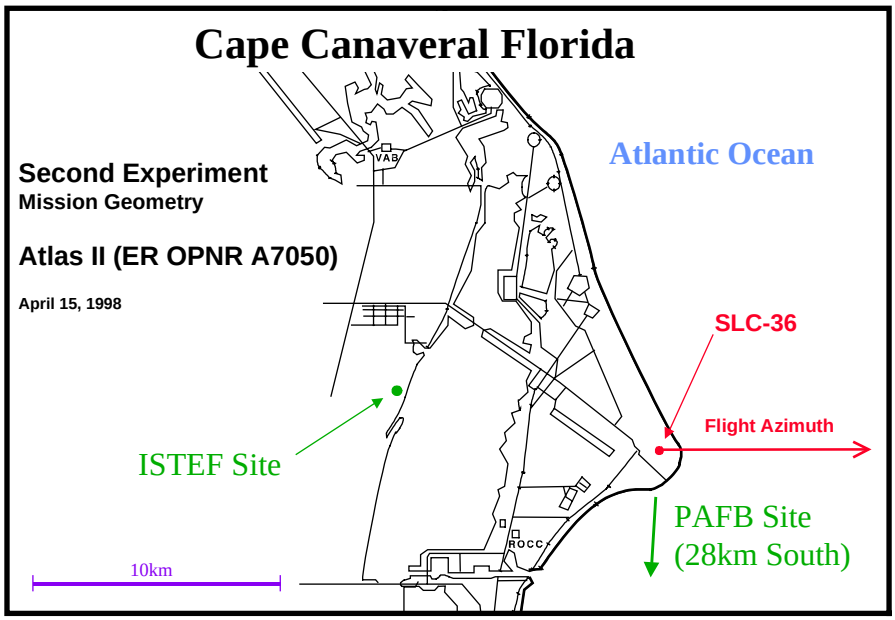

Figure 6 - Mission Geometry for Second Mission

3.1. The Location

Figure 6 shows the launch geometry for the Second Experiment. The laser and passive sensors were located at the ISTEF site, which is at a distance of approximately 11km from the launch point. A second mount (Figure 7) was located at a site approximately 50km south of the launch site, at Patrick Air Force Base (PAFB). This mount hosted a number of cameras covering wavebands from UV to LWIR. Since the Atlas rocket flew eastward, the ISTEF site only collected about 120 seconds of data laser backscatter data before the rocket reached 180 degrees aspect, at which time we terminated track. However, the PAFB tracking mount saw a much better target aspect and collected passive data until the target elevation less than 1 degree above the horizon.

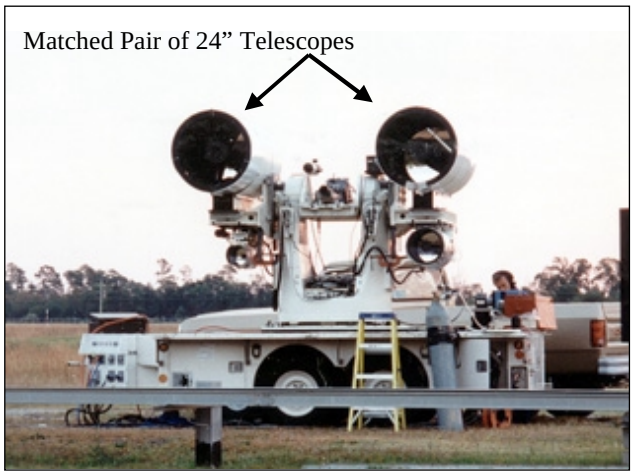

Figure 7 - KTM Tracking Mount

3.2. The Laser System

The Laser system used on the Second experiment was nearly identical to that used on the First Experiment with several exceptions. First the output energies were 0.43 J/pulse at 532m and 0.09J/pulse at 1064nm. Second, a new APD was procured which dramatically increased the sensitivity at 1064nm. Third, the fiber optic attenuator (Figure 5) was modified to improve precision and accuracy. Finally, the digitizer speed was increased to 1GHz for both 532n and 1064nm.

3.3. The Passive Sensors Complement

On the First Experiment, none of the passive sensors were radiometrically calibrated. For the Second Experiment, we added radiometrically calibrated passive sensors to both the GRAZ mount at the ISTEF site and the KTM mount at the PAFB site.

OPTIC NAME	APERTURE	FOCAL LENGTH	CAMERA	BANDPASS	RECORD METHOD	RADIOMETRIC CALIBRATION
GRAZ Main	20”	480”	Xybion ICCD	visible	SVHS	NO
Zoomar	5”	40”	Panasonic CCD	532nm (3nm notch filter)	SVHS	NO
Meade	8”	80”	Panasonic CCD	532nm (3nm notch filter)	SVHS	NO
Wide Angle	2”	8”	Sony CCD	Visible	SVHS	NO
Celestron	4”	30”	Amber MWIR	3-5 microns	12bit Digital	YES

Table 2 – Passive Cameras for Second Experiment at ISTEF Site

3.3.1. Graz Mount at ISTEF Site

Table 2 shows the passive sensor complement of the GRAZ mount at the ISTEF site. One of these sensors, the Amber MWIR camera, was radiometrically calibrated. This camera was configured with a 3.6-3.8 micron band pass filter and 1.0 ND filter that were manually removed during the observation. This sensor was used with Celestron Newtonian optics with 29.5 inch focal length to provide a moderate field of view in order to observe the entire plume.

The MWIR camera digital output was digitally recorded with 12bit resolution. The remaining sensors were recorded on SVHS tape, which was encoded with IRIG B (UTC) time on one audio channel. All imaging sensors were *metrically* calibrated to provide good angle-angle data so the 3D position of the target could be determined..

3.3.2. KTM Mount at PAFB Site

Table 3 shows the passive sensor complement of the KTM mount at the PAFB site. Four of these sensors: the Amber MWIR camera, the JPL QWIP LWIR, the Sony NIR and the Xybion UV ICCD were radiometrically calibrated. The four cameras were arranged in pairs on the 24" aperture telescopes (Figure 7) using splitters. The MWIR and LWIR cameras shared one telescope and the NIR and UV cameras shared another telescope. Since the two 24" aperture telescopes are identical, all four wavebands have the same field-of-view. This ability to field four calibrated wavebands bands (LWIR, MWIR, visible-NIR and UV) with matched fields-of-view is unique to the BMDO/ISTEF.

OPTIC NAME	APERTURE	FOCAL LENGTH	CAMERA	BANDPASS	RECORD METHOD	RADIOMETRIC CALIBRATION
24" number 1	24"	200"	Xybion ICCD	UV (several bands)	VHS	YES
24" number 1	24"	200"	Panasonic CCD	NIR	SVHS	YES
24" number 2	24"	200"	Amber MWIR	MWIR (3.7 micron)	12 bit Digital	YES
24" number 2	24"	200"	JPL QWIP	LWIR	12 bit Digital	YES
Questar	7"	120"	Panasonic CCD	Visible	SVHS	NO
Davro	12"	120"	Panasonic CCD	Visible	SVHS	NO
Wide Angle	2"	8"	Sony CCD	Visible	SVHS	NO

Table 3 – Passive Cameras for Second Experiment at ISTEF Site

The MWIR camera was filtered to a narrow band centered on 3.7 microns. Additionally, 0.6 and 0.3 Neutral Density filters were used to control the FPA irradiance. Field calibration data was taken before and after the launch.

The LWIR sensor was a JPL QWIP in a Radiance/4256 hybrid configuration on loan from JPL. The sensor was configured with four fixed offset and gain setups to cover the expected irradiance range. No filters were used, giving a bandbass of approximately 8-9 microns. This sensor was calibrated post-mission.

The NIR camera was operated in a single fixed gain configuration with a band pass of approximately 0.8 to 1.1 micron.

The UV-VIS Sensor had a filter wheel which was manually commanded to switch between four filters: 310nm, 390nm and 488nm band pass, and a 400nm long wave pass cut on filter.

4. The Data

During the First Experiment both active and passive data was collected. However, we will omit discussion of the passive data here since it was not calibrated.

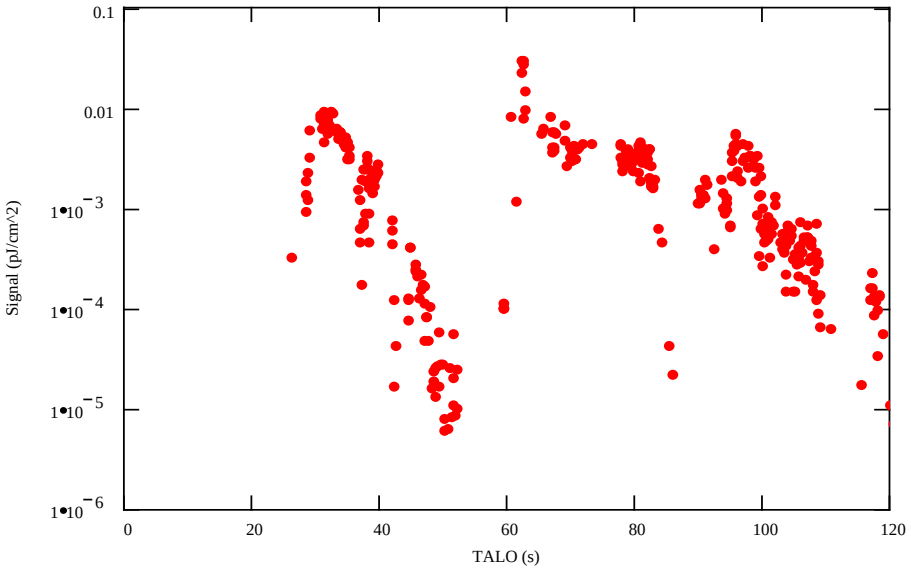

Figure 8 - First Experiment: 532nm Irradiance

4.1. A0116

4.1.1. Laser Target Backscatter Data

Figures 8 and 9 show the calibrated irradiances (in pJ/cm^2), at the receiver aperture, for both 532nm and 1064nm. The calibration of this backscatter data was made difficult by the fact that the irradiances on the receiver covered 6 orders of magnitude. At the time of the writing of this paper, we have not completed the error analysis. We do however believe that the errors are on the order of 15%-20%. The largest errors coming from the atmospheric absorption model for the Spectralon (1km) field calibration.

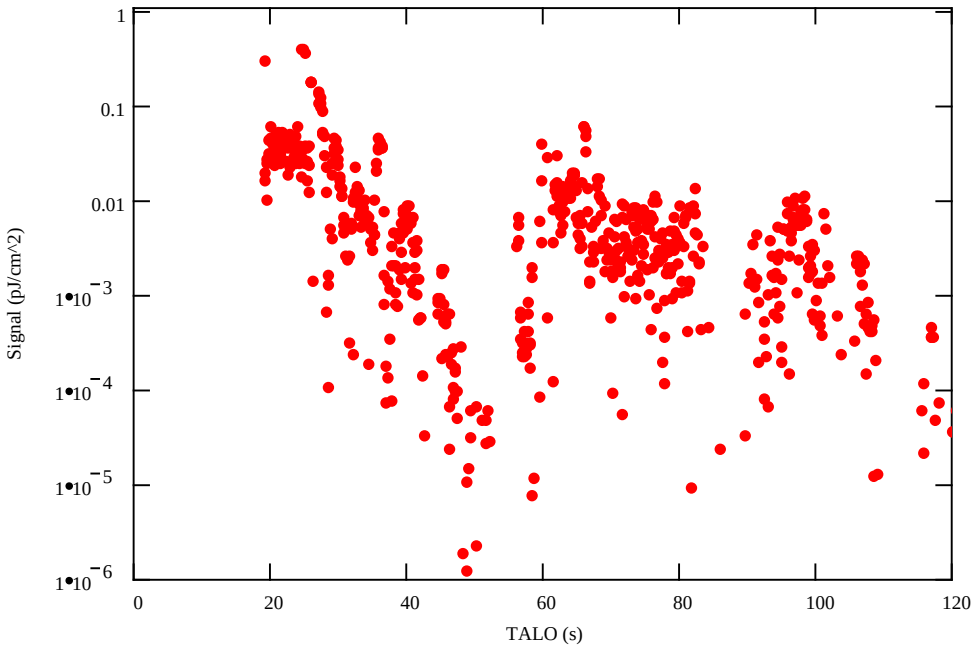

Figure 9 - First Experiment: 1064nm Irradiance

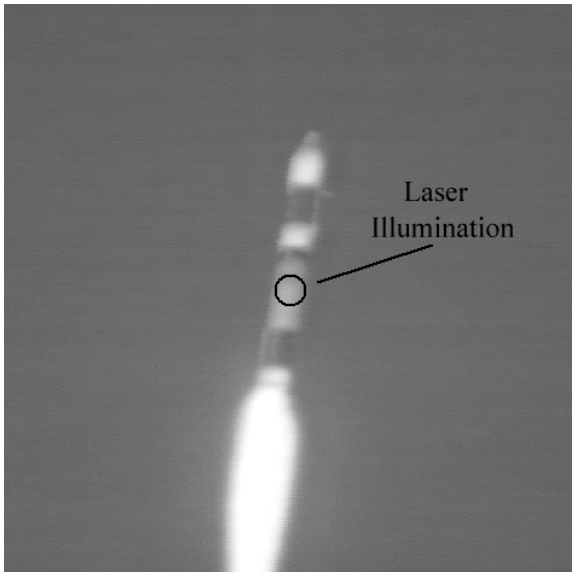

Figure 10 – 30s TALO

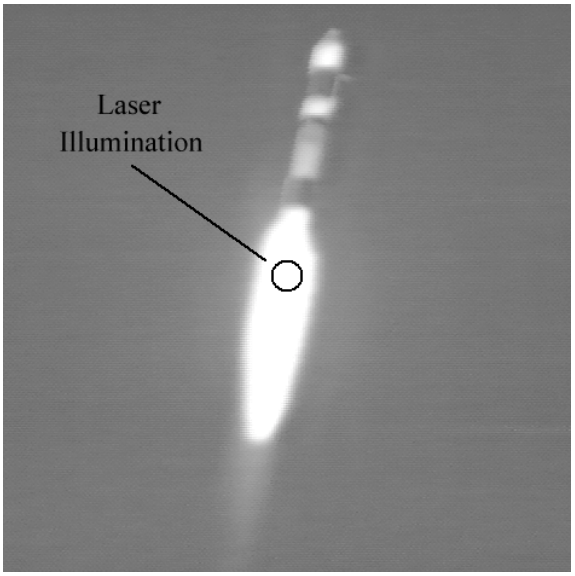

Figure 11 – 40s TALO

During the data collection, the beam was twice scanned from the plume to the hardbody to aid in calibrating out the atmospheric effects. Figure 10 shows the illumination spot of the laser on the hardbody at 30 seconds TALO. Figure 11 shows the illumination spot on the plume at 40 seconds TALO. A detailed time line for this launch, giving aim point relative to the nozzle exit plane as a function of time, is available.

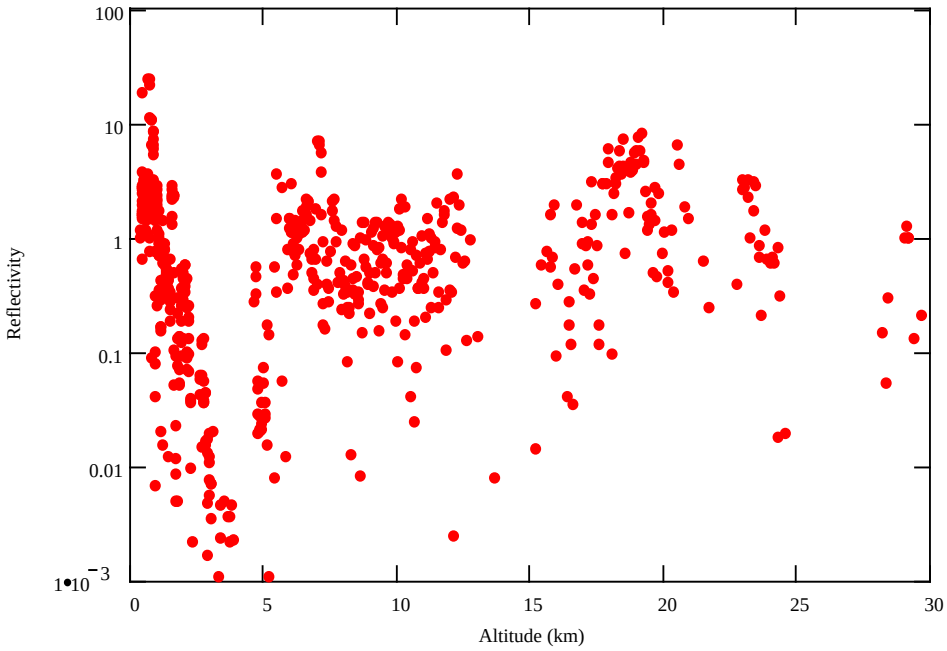

Figure 12 - First Experiment: 1064nm Reflectivity

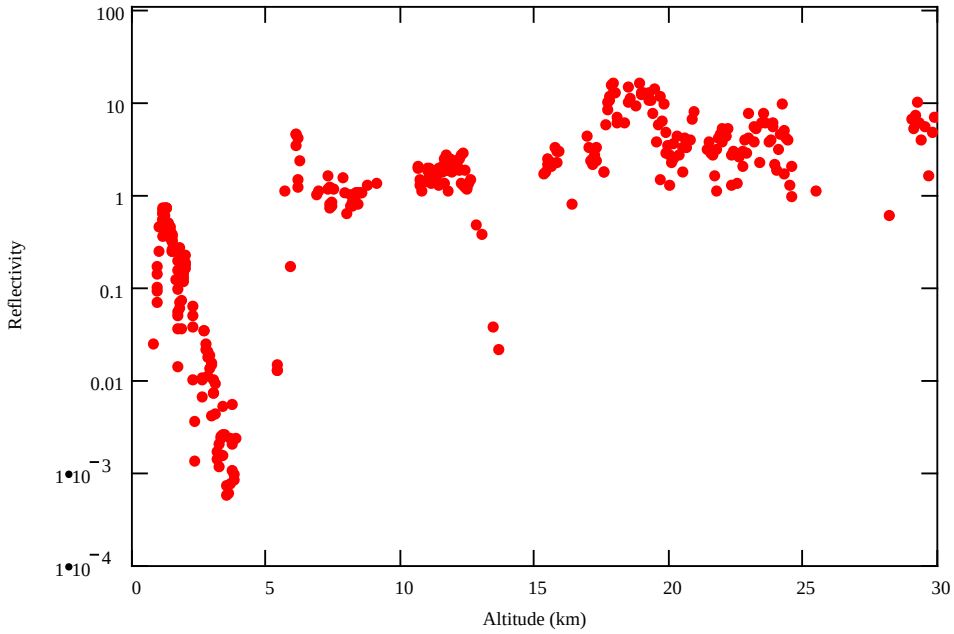

Figure 13 - First Experiment: 532nm Reflectivity

We used an atmospheric model based on Lowtran and Fastcode profiles for the atmosphere to determine the hardbody and plume reflectivities at both wavelengths. By reflectivities we mean the total integrated backscatter for the plume and the diffuse reflectivity for the hardbody. The results are shown, versus altitude, in Figures 12 and 13.

It is clear from these figures that the cross sections (reflectivities) are too high. This is due to problems with the atmospheric model and not with the system calibration. Still, you can clearly see the cross

section fall off between 1km and 4km altitude as the laser beam was scanned down the plume from the nozzles until loss-of-signal. Also notice the area of constant cross section between 7km and 8km altitude where the beam was held steady on a spot about 10m down from the nozzles. Figure 14 shows the results from a 4-second scan from the nozzle plane to loss of signal at 140m downstream from the nozzles. The data points shown are the 532nm backscatter signal. The vertical dimension has been scaled to fit 0-100. The solid line is a graph of plume radiance (also scaled to fit 0-100) at approximately the same altitude, but from the Second Experiment. We must be careful about drawing conclusions since the LRCS data and the plume radiance data are from different launches but it is suggestive that as the soot cross section falls off so does the plume radiance. This behavior of the plume radiance has been observed numerous times by BMDO/ISTEF.

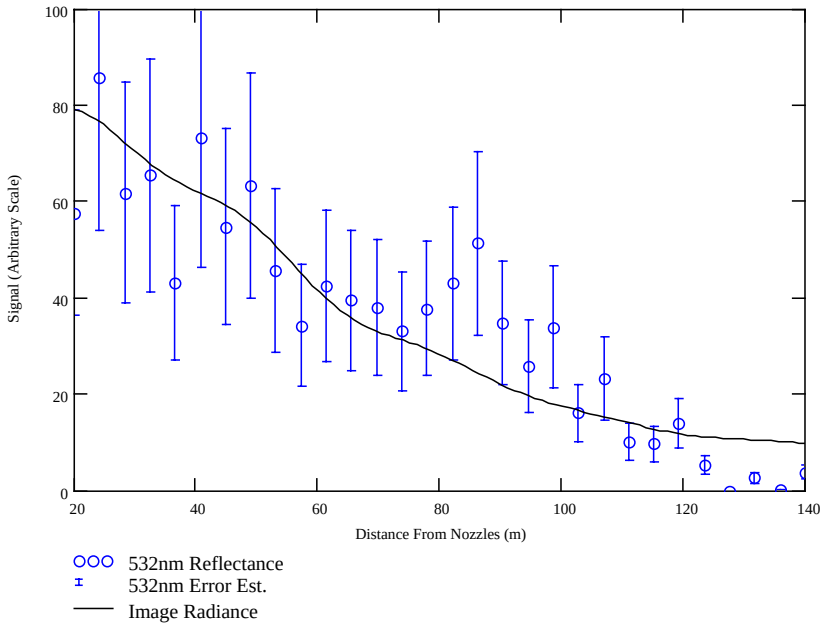

Figure 14 - Longitudinal Plume Scan

At this time our analysis is not complete since, in addition to the problems with the atmospheric model, we did not fully account for the details of the target geometry (illumination function, aspect angle). In a follow-up paper, an improved analysis will be presented. The analysis presented here is only to help the reader better understand the value of the data.

Finally, we want to be clear that the irradiances at the aperture quote above are accurate and calibrated.

4.2. A7050

The data collected on the Second Experiment is much better than that collected on the First Experiment, mainly owing to the improved data collection.

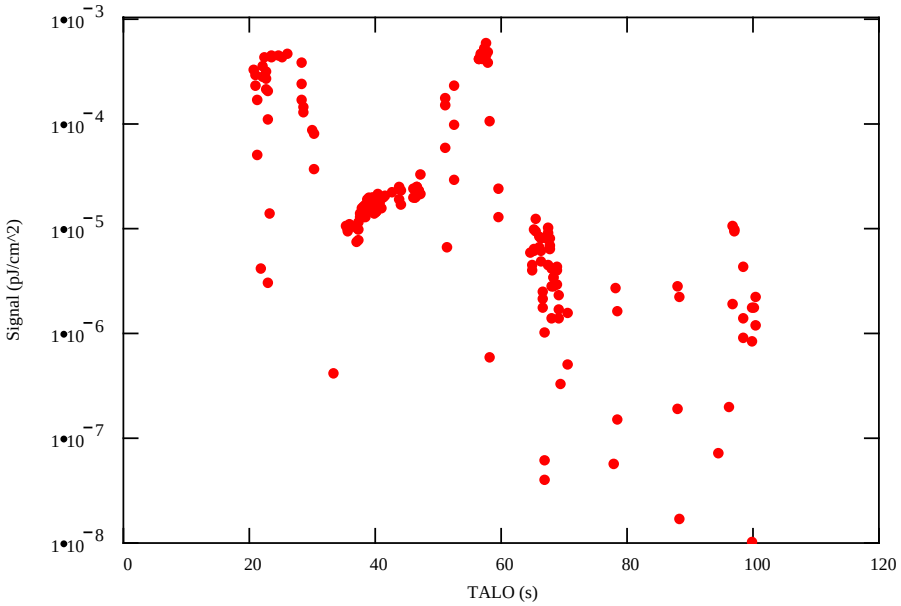

Figure 15 - Second Experiment: 1064nm Irradiance

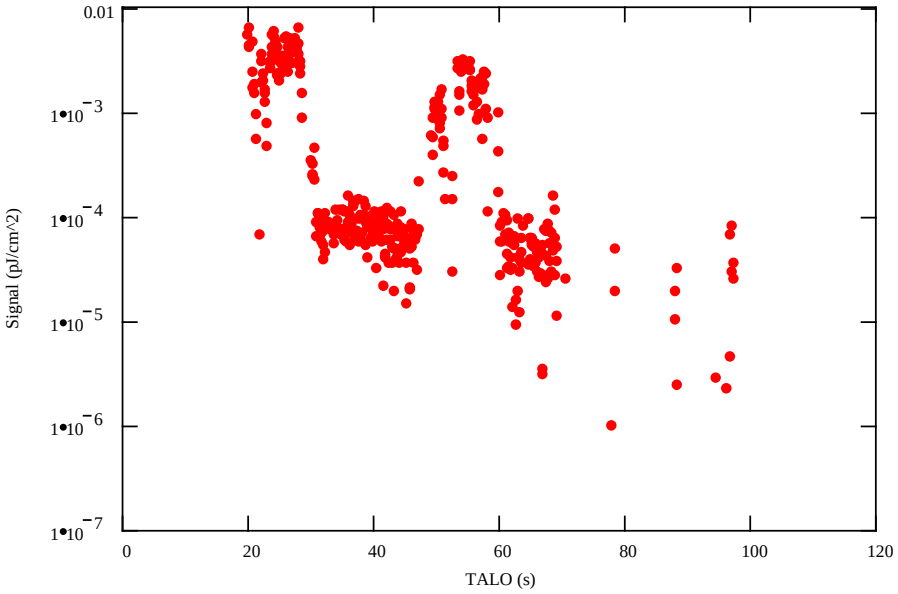

Figure 16 - Second Experiment: 532nm Irradiance

4.2.1. Laser Target Backscatter Data

Figures 15 and 16 show the calibrated irradiances (in pJ/cm^2), at the receiver aperture, for both 532nm and 1064nm. As mentioned above the calibration was accomplished by using a Spectralon target at a distance of 1km (in the far field). At the time of the writing of this paper, we do not have the error analysis complete. We do however believe that the errors are on the order of 10%-15%. The largest errors coming from the atmospheric absorption model for the Spectralon (1km) field calibration.

As in the First experiment, the beam was twice scanned from the plume to the hardbody during the data collection to aid in calibrating out the atmospheric effects. Unlike the First Experiment, the beam was not scanned down the plume, but was aimed at a specific point downstream from the nozzles. A detailed time line for this launch, giving aim point relative to the nozzle exit plane is available.

The same atmospheric model used above was applied to this data and the results are shown in Figures 17 and 18. Once again the reflectivities are defined as the total integrated backscatter for the plume and the diffuse reflectivity for the hardbody.

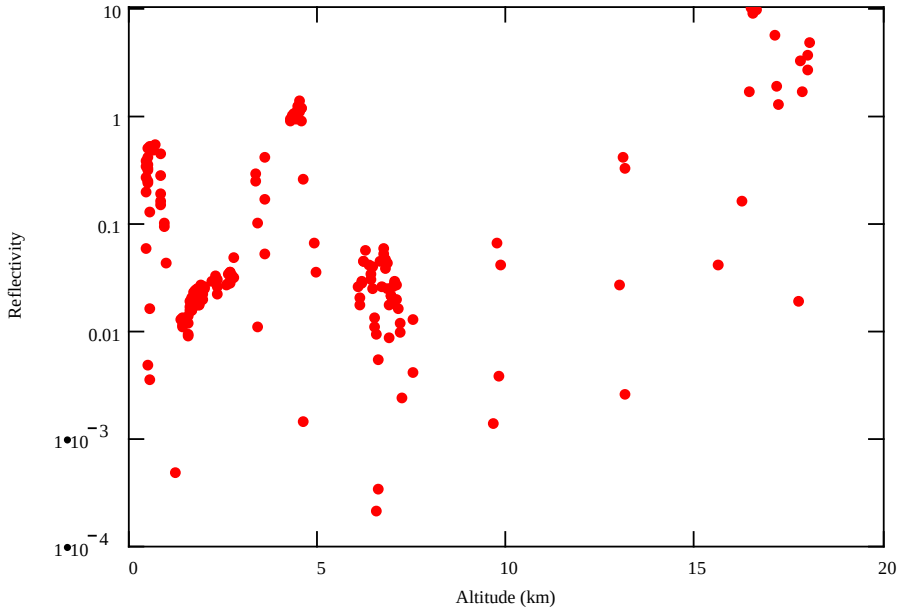

Figure 17 - Second Experiment: 532nm Reflectivity

It is clear from these figure that the data from this mission is more consistent that from the First Experiment. The two hardbody collects are clearly visible as the peaks centered a 1km and 4 km altitude.

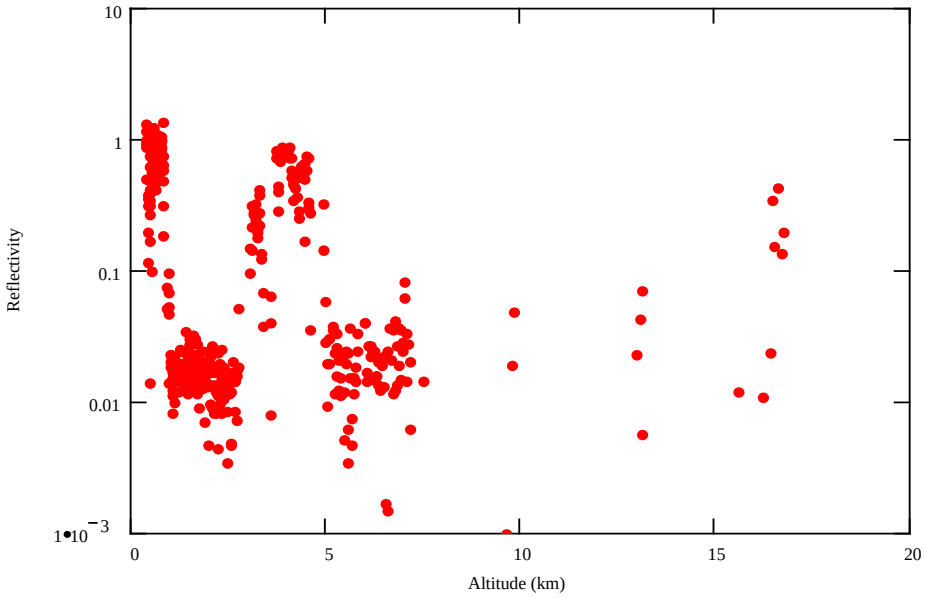

Figure 18 - Second Experiment: 1064nm Reflectivity

From these figures we see that the reflectivities at both wavelengths are down from the hardbody reflectivity by almost 2 orders of magnitude. In our analysis, the target geometry was not taken into account and doing so will further improve the results. However, since the illumination functions for 532nm and 1064nm beams are the same at the target, we may ratio the reflectivities to cancel out the effects of the target geometry (figure l9).

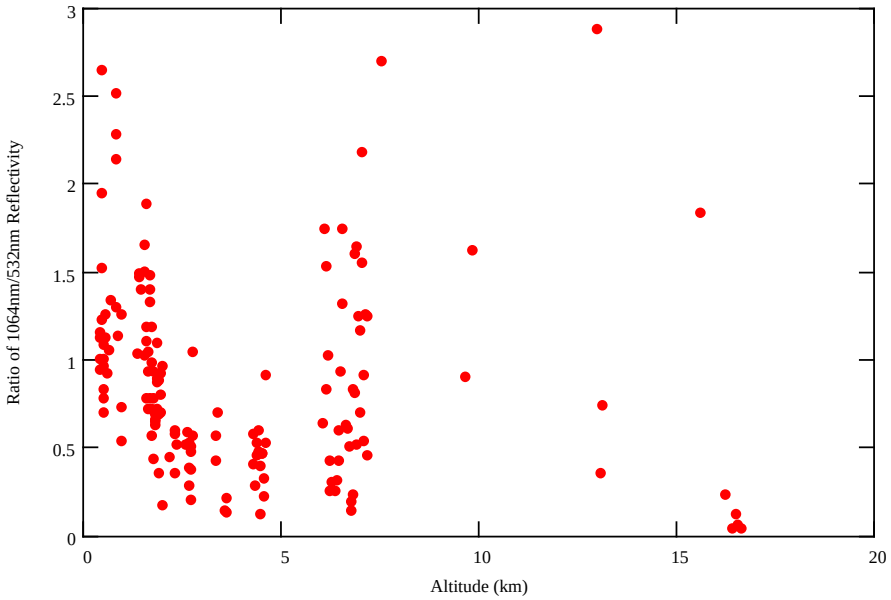

Figure 19 - Second Experiment: Reflectivity Ratio

One thing is immediately apparent. The scattering is not Rayleigh scattering. If it were, the ratio above would be 1/16 or 0.0625. This puts a definite constraint on the minimum size of the soot grains.

Finally, we want to point out another valuable feature of this laser backscatter data: namely, the high temporal resolution. Figure 20 shows a single raw digitizer trace from the first plume track at approximately 2 km altitude.

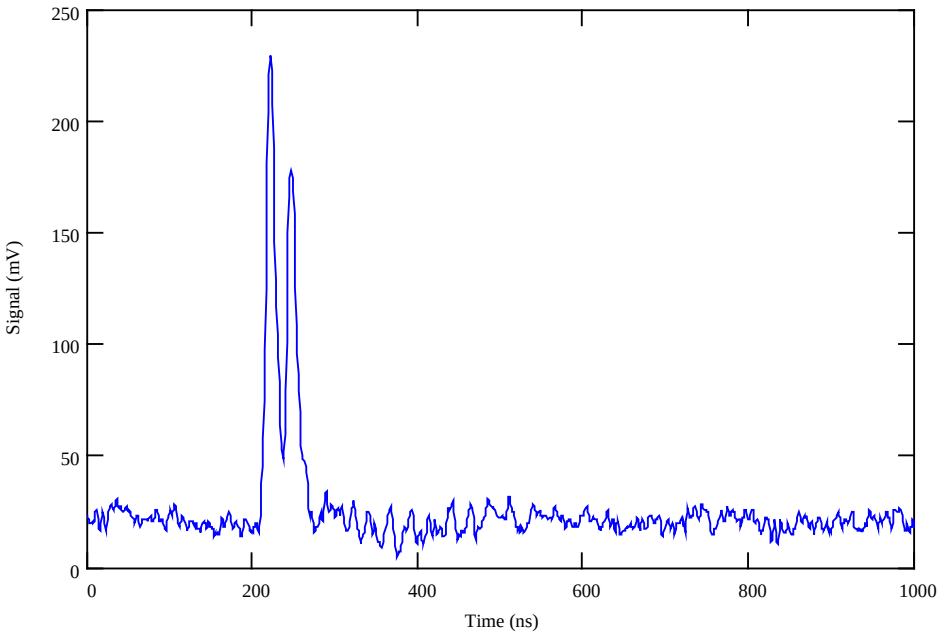

Figure 20 - Raw 532nm Signal from Digitizer

The two clearly visible peaks are the returns from the two booster engines of the Atlas II. The distance between the two peaks corresponds to the spacing of the two engines since, from the ISTEF Site the laser beam lies nearly in the plane formed by the two plumes. This high resolution data along with the passive data, shown in the next section, forms a complete set of high spatial resolution, active and passive signatures on a surrogate threat target.

4.2.2. Passive FPA Data

Figure 21 show some sample four-band radiance data collected from the KTM tracking mount at PAFB. The data is from approximately T+70 seconds. This is high spatial resolution data that complements the laser data taken from the ISTEF site. The line-of-site from PAFB site was almost perpendicular to the line-of-sight from ISTEF. Calibrated MWIR radiance data was also measured from the ISTEF site during the Second Experiment.

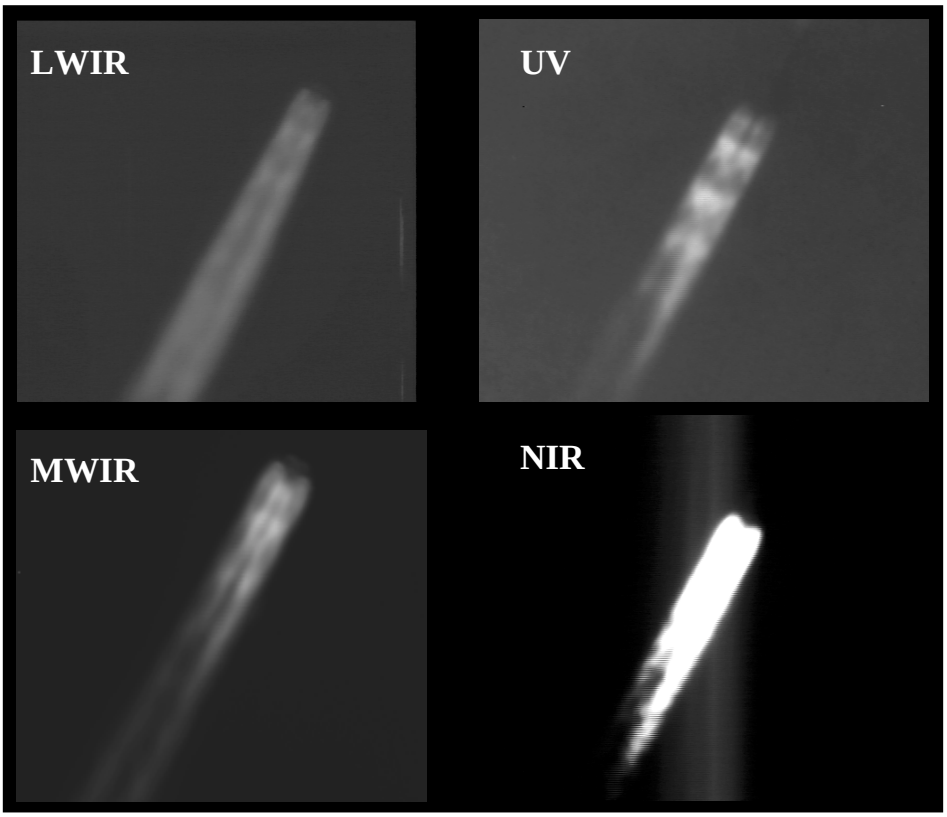

Figure 21 - Sample Multi-Band Radiance Data

4.3. Future Experiments

Over the next year ISTEF plans a number of additional collections to improve the signature database. Future experiments will incorporate a number of improvements to the laser system and data recording system. Additionally, the atmospheric calibration will be improved by collected atmospheric backscatter data for every laser pulse. Finally, we will add a second *transportable* laser system on the next test. This last improvement will allow us to fully support BMDO launches at locations other than Cape Canaveral.

5. Conclusions

Three important observations were made. First, from the Second Experiment we saw that the plume reflectance (integrated backscatter) is down 2 orders of magnitude below the hardbody signature (Figures 15,16). This may have implications for target identification and aim point selection. Second, We saw from the plume scan data that the cross section fell to zero (immeasurable) at the same rate as the plume radiance (Figure 14). This may help us to better understand the effects of soot on the chemistry and hence, the ***in-situ*** signature of plumes. Finally, the ratios of reflectances at the two wavelengths may help plume modelers put bounds on the soot particle size distribution.

Lastly, ISTEF plans to make more ***in-situ*** measurements of soot backscatter over the next year, including collections from locations other than Cape Canaveral.

This paper demonstrates a unique capability of the BMDO ISTEF Site, the ability to collect ***in-situ*** active and passive signature data from treat representative targets**.** To our knowledge this ability is unique. We have presented high quality dual-wavelength laser backscatter measurements along with calibrated multi-waveband passive FPA radiance data. Though the data analysis presented here is preliminary and incomplete, it shows the great value of these data sets to the plume phenomenology and target signature communities.

6. Acknowledgements

This work was performed under BMDO contract N68001-98-D-0088. The authors would like to acknowledge contributions of the ISTEF passive sensors group and in particular Jody Wendt for providing the radiance data presented in this paper.